

## A Novel Twist Deformation Model of Soft Tissue in Surgery Simulation

Xiaorui Zhang<sup>1,2,3,\*</sup>, Pengpai Wang<sup>1</sup>, Wei Sun<sup>2</sup> and Norman I. Badler<sup>3</sup>

**Abstract:** Real-time performance and accuracy are two most challenging requirements in virtual surgery training. These difficulties limit the promotion of advanced models in virtual surgery, including many geometric and physical models. This paper proposes a physical model of virtual soft tissue, which is a twist model based on the Kriging interpolation and membrane analogy. The proposed model can quickly locate spatial position through Kriging interpolation method and accurately compute the force change on the soft tissue through membrane analogy method. The virtual surgery simulation system is built with a PHANTOM OMNI haptic interaction device to simulate the torsion of virtual stomach and arm, and further verifies the real-time performance and simulation accuracy of the proposed model. The experimental results show that the proposed soft tissue model has high speed and accuracy, realistic deformation, and reliable haptic feedback.

**Keywords:** Kriging interpolation method, membrane analogy, twist deformation, virtual soft tissue, surgery simulation.

### 1 Introduction

Medicine is, to some extent, an empirical subject, especially for surgery. Doctors need not only solid medical theory, but also abundant clinical experience. Therefore, it is an urgent task to train more outstanding young surgeons in a shorter period with better effects and lower cost. However, the perfection of a surgeon is not able to be accomplished in a day, but a result of long-term practice. Based on current training methods and technical conditions, it will take approximately 8-10 years to become a seasoned surgeon. Virtual surgery system can simulate various surgical operations, shorten the training period for surgeons, and improve operating skills. It is not only helpful in alleviating the shortage of surgeons at present, but also of great significance for constructing a better relationship between doctors and patients.

Using virtual haptic interaction in the process of twist deformation in surgery is very common, in which a good deformation model is the key to success. Meanwhile, the real-time performance and accuracy of soft tissue deformation directly determine the success

---

<sup>1</sup> Jiangsu Engineering Center of Network Monitoring, Nanjing University of Information Science & Technology, Nanjing 210044, China.

<sup>2</sup> Jiangsu Collaborative Innovation Center of Atmospheric Environment and Equipment Technology (CICAET), Nanjing University of Information Science & Technology, Nanjing 210044, China.

<sup>3</sup> School of Engineering and Applied Science, University of Pennsylvania, Philadelphia, 19104, United States.

\* Corresponding author: Xiaorui Zhang. Email: zxr365@126.com.

of virtual surgery. Among the current deformation models, Benítez et al. [Benítez and Montáns (2017)] simulated the skin with the finite element model by applying nonlinear behavior and anisotropy, but the model will lead to unstable element deformation when there is a large acceleration. As a result, it is not suitable for simulations with large or fast deformation. Besides, with the numbers of element nodes increasing, it is difficult to guarantee the real-time performance of the system.

Spranger et al. [Spranger, Capelli, Bosi et al. (2015)] designed a virtual vascular stenting based on mass-spring model, which can simulate blood vessel deformation. During deformation, genetic algorithm is used to quickly determine the parameters used in the finite element model. The algorithm not only retains the advantages of the mass-spring model, such as model simplicity and small amount of calculation, but also overcomes the difficulties in the decrease of precision. However, when the cylinder of soft tissue becomes large, node localization error will occur inevitably and the simulation precision will also decrease. Kim et al. [Kim, Chang, Kim et al. (2013); Zhang, Gao, Yan et al. (2016)] used the mixed model of boundary element, finite element and mass spring models to simulate resect of gallbladder. However, too many models were utilized during the deformation simulation, which leads to a rather low accuracy of deformation. Meanwhile, deformation error occurs easily in the joint area between different models.

This paper presents a novel twist model based on the Kriging interpolation method and membrane analogy method. The Kriging interpolation method can control its accuracy by adjusting the weighted values. The membrane analogy method models the soft tissue surface under external force as a thin membrane. The integration of Kriging interpolation and membrane analogy method can accurately determine the twisting displacement after deformation. It can reduce the deformation time of the model and meet the real-time requirement of virtual interaction. We test the proposed model based on comprehensive performance evaluations and the experimental results demonstrate the advantages of our method.

The contributions of this study can be summarized as follows. Firstly, the Kriging interpolation method is used to can accurately determine the deformed position of the points in the soft tissue deformation process. Secondly, the proposed membrane analogy method can stretch the membrane on a hole similar to the cross section of torque. It makes the computation and analysis of twist deformation become more intuitive and improves the model accuracy under large-scale deformation. Thirdly, in order to verify the practicability of the proposed model, we propose a weighted comprehensive evaluation method based on several typical indicators. The typical indicators are designed according to the demands of practical surgery training.

The remainder of this paper is organized as follows. Section 2 describes the Kriging interpolation and membrane analogy method. Section 3 proposes the deformation algorithm based on the Kriging interpolation and membrane analogy method. Section 4 presents the details about the constructed experimental platform. Section 5 shows implementation and results in stomach and arms as well as analysis of experimental results. Some concluding comments and some suggestions for future work are provided in Section 6.

**2 Prior knowledge**

In this paper, in order to increase accuracy of soft tissue twist operation and decrease computational complexity of twist simulation, the Kriging interpolation method is used to interpolate the deformation between sampling points, and the membrane analogy method is utilized to compute the variation of the marked points. Using ridge and parallel to the bottom surface formation intersection point in column model of soft tissue. It is defined as the key sample point. The key sample point adjacent regions were interpolated by Kriging interpolation method. The film crated from four contiguous intersections using membrane analogy method to force analysis, the final position in space after deformation.

**2.1 Kriging interpolation method**

The Kriging interpolation method is an optimal interpolation method, it can estimate the values of interpolation points in the region near the determined points by using the values of the determined points [Chen, Liu, Li et al. (2016)]. The points of soft tissue under twist deformation belong to the spatial variables, as a result, Kriging interpolation method can be used to interpolate them quickly and accurately. It takes the spatial relationship between interpolation points and key points into account. It is suitable for spatial interpolation and can improve the accuracy of the twist deformation of soft tissue.

The prerequisite for Kriging interpolation is that there are similarities for these points in adjacent space regions [Dehghan and Abbaszadeh (2017)].  $Z(x)$  is the observed value of sampling points  $x$ , the variable  $Z(x)$  consists of expectation value  $c$  and residual value  $E(x)$ , as is shown in Eq. (1):

$$Z(x) = E(x) + c \tag{1}$$

where the expectation value  $c$  is unknown and the expectation of residual value  $E(x)$  is zero.

The stationarity assumption of  $Z(x)$  satisfies the following equations:

$$E[Z(x+h) - Z(x)] = 0 \tag{2}$$

$$Var[Z(x+h) - Z(x)] = 2\gamma(h) \tag{3}$$

where  $\gamma(h)$  is a variogram.

The Kriging interpolation can be described by Eq. (4):

$$Z^*(x_0) = \sum_{i=1}^n \lambda_i Z(x_i) \tag{4}$$

where  $Z^*(x_0)$  is the estimated value of the position  $x_0$ ,  $Z(x_i)$  is the observed value of sampling points  $x_i$ ,  $\lambda_i$  is the weight of  $Z(x_i)$ , and  $n$  is the number of the observed value.

Kriging interpolation method satisfies the following equations:

$$\begin{cases} \sum_{j=1}^n \lambda_j C(x_i - x_j) - \mu = C(x_i - x_0), i = 1, 2, \dots, n \\ \sum_{i=1}^n \lambda_i = 1 \end{cases} \tag{5}$$

where  $C(x_i - x_j)$  is the covariance between  $x_i$  and  $x_j$ , which is determined by the unbiased estimation error and variance of minimum estimation error.

The assumption of the unbiased estimation should satisfy  $E[Z^*(x_0) - Z(x_0)] = 0$ .

Based on the Eq. (5), the assumption above can be formulated as:

$$\left(\sum_{j=1}^n \lambda_j - 1\right)E[Z(x_0)] = \left(\sum_{j=1}^n \lambda_j - 1\right)c = 0 \quad (6)$$

The above equation holds for any given  $c$ , so the unbiased estimation can be further simplified into Eq. (7).

$$\sum_{j=1}^n \lambda_j = 1 \quad (7)$$

The variance  $\sigma_o^2$  of estimated error is:

$$\begin{aligned} \sigma_o^2 &= \text{Var}[Z^*(x_0) - Z(x_0)] \\ &= \sum_{i=1}^n \sum_{j=1}^n \lambda_i \lambda_j C(x_i - x_j) - 2 \sum_{i=1}^n \lambda_i C(x_i - x_0) + C(0) \end{aligned} \quad (8)$$

In order to minimize the variance, we compute the partial derivative of the variance with respect to  $\lambda_j$  and make it equal to 0. Because  $\lambda_i$  satisfies  $\sum_{i=1}^n \lambda_i = 1$ , we can use the

Lagrange multiplier method to solve the equation [Tu, Dong, Yang et al. (2016)].

Then the Kriging interpolation is finally calculated as follows:

$$Z^*(x_0) = \sum_{i=1}^n \lambda_i Z(x_i) \quad (9)$$

## 2.2 Membrane analogy

The membrane analogy method can be used to analyze the force on the surface of soft tissue by modeling the surface as a membrane [Troyani, Pérez, Gomes et al. (2009)], then the deformation and stress analysis is carried out through membrane analogy method. Elastic film can be posted on the surface of the project and have similarity with twisting and bending [Liu, Yu, Shen et al. (2016)]. The unknown variables in the model of twist and bending can be determined by studying the membrane. The force analysis of the small membrane makes the computation and analysis of the soft tissue under spatial twist more convenient and simple, which improves the deformation accuracy and efficiency of the model.

Assuming a homogeneous and isopachous membrane is tightly attached to a hole that is similar with the interface of the twisted bar in the shape, as shown in Fig. 1. A symmetrical pressure  $q$  is applied to one side of the membrane, and the membrane is subjected to a symmetrical tension  $S$ . When the deformation is very little in membrane,

the resultant force in the direction  $z$  applied to the  $ab$  and  $ac$  sides of the microcell  $abcd$  is  $S\left(\frac{\partial^2 z}{\partial y^2}\right)dydx$ .

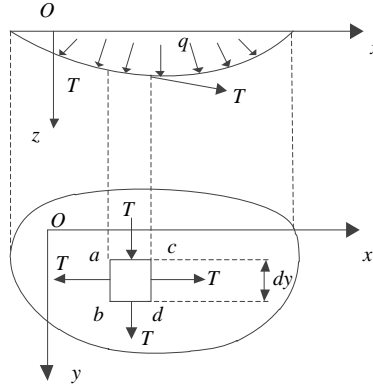


**Figure 1:** Membrane analogy

Similarly, the resultant force on the  $bd$  and  $cd$  sides of the unit are  $S\left(\frac{\partial^2 z}{\partial x^2}\right)dxdy$  in the  $z$  direction, the equilibrium equation of the unit is:

$$S\left(\frac{\partial^2 z}{\partial y^2}\right)dydx + S\left(\frac{\partial^2 z}{\partial x^2}\right)dxdy + qdxdy = 0 \tag{10}$$

which is equivalent to:

$$\frac{\partial^2 z}{\partial x^2} + \frac{\partial^2 z}{\partial y^2} = -\frac{q}{S} \tag{11}$$

Because the membrane's sag at the boundary is zero, the stress function  $\Phi$  of the membrane is obtained [Yang, Yuan and Zhao (2017)]:

$$\Phi = \frac{2G\theta}{q} z \tag{12}$$

where  $G$  is shear modulus and  $\theta$  is twisting angle.

### 3 Method

The twist model in this paper is based on the Kriging interpolation and the membrane analogy method. In the process of twist operation, the cylinder surface is firstly partitioned into small grids, and then unknown points are determined by Kriging interpolation method based on the sample points. Kriging interpolation method makes full use of spatial positions of both interpolation points and sample points, which leads to better performance in spatial interpolation and higher accuracy.

### 3.1 The cartesian coordinate system of establishment

First, a spatial Cartesian coordinate system is established to describe the small changes in the entire cylinder under torque.

Assumed that there is an elastic cylinder with irregular cross section, the upper end is the free end, and the lower end is the fixed end [Surkay and Mahir (2018)]. The horizontal plane of the fixed end is set as the  $XY$  plane and the center axis of the lower end face perpendicular to the fixed end is set as the  $Z$  axis, spanning  $XYZ$  space Cartesian coordinate system. The origin  $O$  is the fixed end of the center point. In the side of the irregular cross section cylinder,  $N$  parallel and equidistant ridges are selected, the range of  $N$  is from 2 to 360. We select  $M$  cross sections parallel to the upper and lower end, including the upper and lower end of the cross section, and the vertical distance between adjacent sections equals, the range of  $M$  is from 2 to 360, the flow chart is shown in Fig. 2.

We regard the intersection of each section and each line as the key sample point, the intersection line of cross section and the ridge line as the cross-section line, and set the ridge as meridian, the section line as the weft. The adjacent warp and weft divide the sides into a series of block areas, let  $S$  be the number of blocks of the divided side, we have:

$$S = (M - 1) \cdot N, \quad M = 2, 3, 4 \dots 360, \quad N = 2, 3, 4 \dots 360 \quad (13)$$

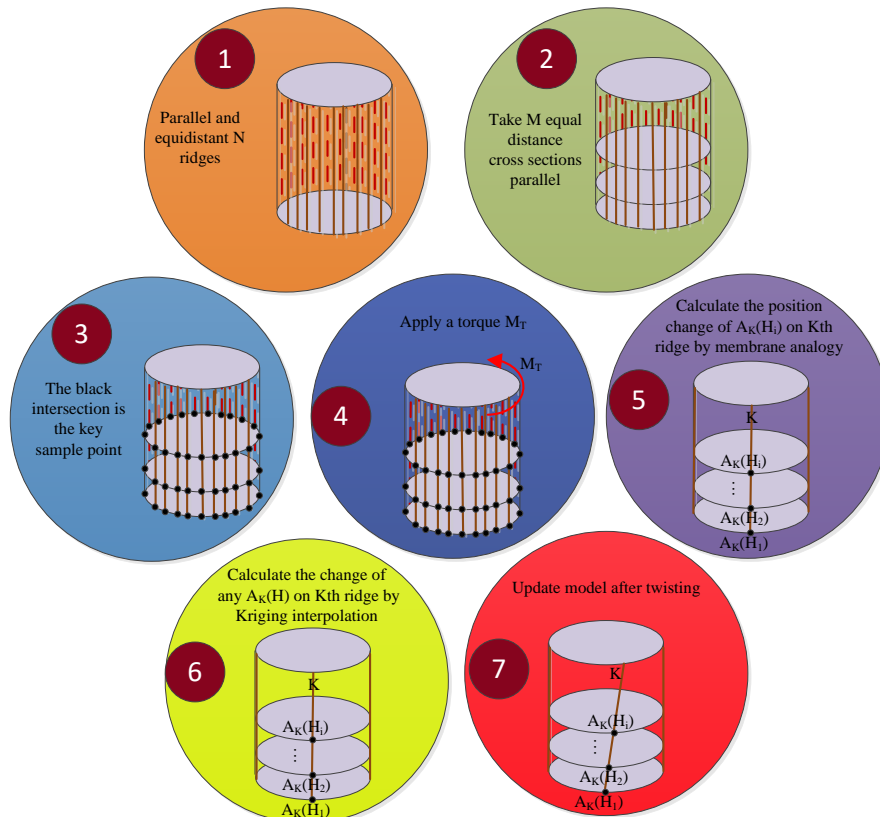


Figure 2: Modeling process

### 3.2 The key sample mark point

We set the grid intersection on the cylinder as a key sample point and mark it with the Kriging interpolation method discretely.

Assuming that the intersection of any  $K^{th}$  row and  $M$  cross sections on the side is a key sample point, we show the distribution of key sample points on the ridge of the side in Fig. 3. From the upper end to the lower end, the sample points are recorded as:  $A_K(H_1)$ ,  $A_K(H_2)$ ,  $A_K(H_3)$ , ...,  $A_K(H_i)$ , ...,  $A_K(H_M)$ .

It is assumed that a random torque  $M_T$  is applied to the upper end face. Under the influence of moment, any key sample point  $A_K(H_i)$  on the  $K^{th}$  ridge line has three varying quantities, which are  $\Delta X_{A_K}(H_i)$ ,  $\Delta Y_{A_K}(H_i)$  and  $\Delta Z_{A_K}(H_i)$  in the  $X$ ,  $Y$ ,  $Z$  direction, respectively.

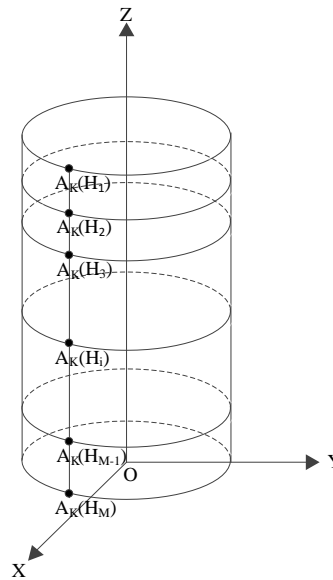


**Figure 3:** Key sample point distribution map

Any estimated point  $A_K(H_i)$  is at any distance  $H$  from the fixed end, the estimated amount of change is  $\Delta X_{A_K}^*(H)$  in  $X$  axis under torque  $M_T$ .

Let  $h$  be the vertical distance from  $A_K(H_i)$  to  $A_K(H_M)$ , i.e. the vertical distance between adjacent key sample points on the  $K^{th}$  ridge, which are all equal. The key sample points normalization is realized in the Kriging interpolation algorithm [Ganganagoudar, Mondal and Prakash (2016a)], then:

$$H_i = i \cdot h \tag{14}$$

According to the Kriging interpolation algorithm:

$$\Delta X_{A_K}^*(H) = \sum_{i=1}^M \lambda_i \Delta X_{A_K}(H_i) \tag{15}$$

where  $\Delta X_{A_k}(H_i)$  is the variation in the  $X$  axis direction under the action of the torque  $M_T$ , and  $\lambda_i$  is the weight of any estimation point  $A_k(H)$  in this ridge on  $X$  axis.

The key to the Kriging interpolation algorithm is the computation of the weight coefficients of  $\lambda_i$ . The weight coefficient must satisfy the two conditions [Ganganagoudar, Mondal and Prakash (2016b)]:

$$\begin{cases} \sum_{j=1}^M \lambda_j c(H_i, H_j) - \mu = c(H_i, H) \\ \sum_{i=1}^M \lambda_i = 1 \end{cases} \quad (16)$$

Where  $\lambda_i$  and  $\lambda_j$  are weight coefficients, the variation  $\Delta X_{A_k}(H_i)$  and  $\Delta X_{A_k}(H_j)$  of the key sample point  $A_k(H_i)$  and  $A_k(H_j)$  in  $X$  axis is the influence weight of the estimate value  $\Delta X_{A_k}^*(H)$  of any estimate point  $A_k(H)$  in this ridge.  $c(H_i, H_j)$  is the variation function between the key sample points  $A_k(H_i)$  and  $A_k(H_j)$  along the axis under the action of the torque  $M_T$  and  $\mu$  is Lagrange coefficient.  $c(H_i, H)$  represents the variation function between variation  $\Delta X_{A_k}(H_i)$  and estimated value of change  $\Delta X_{A_k}^*(H)$  of any point  $A_k(H)$ .

The weight coefficient  $\lambda_i$  can be obtained from the Eq. (4). According to the Eq. (3), the estimated value in  $X$  axis  $\Delta X_{A_k}^*(H)$  can be obtained as the estimated point  $A_k(H_i)$  under the action of the torque  $M_T$ .

Similarly, according to the key sample points normalization and Kriging interpolation, the estimated values in  $Y$  and  $Z$  axis  $\Delta Y_{A_k}^*(H)$  and  $\Delta Z_{A_k}^*(H)$  can be obtained separately from estimated point  $A_k(H_i)$  of the  $K^{th}$  ridge under the action of the torque  $M_T$ .

Applying a torque  $M_T$  to the free end face,  $A_k(H_i)$  is any key sample point of the  $K^{th}$  ridge when  $i = 1, 2, 3, \dots, M$ .

### 3.3 The twist angle of the critical sample point

In order to determine the displacement of each key sample point, it is necessary to determine the direction of its displacement and spatial variation of the twist angle, the membrane analogy method is used to solve it.

Since the equilibrium equation and the twist force function of the membrane analogy method obey the same differential equation and boundary conditions, we can obtain unit length twist angle:

$$\theta_{A_k(H_i)} = \frac{M_T q}{4VGf} \quad (17)$$

where  $q$ ,  $V$ ,  $G$  and  $f$  respectively represent the tiny uniform pressure on the membrane, the cylinder of the membrane corresponding to the force of the elastic cylindrical material, the modulus of elasticity and the tension on the membrane.

There is an exponential relationship between the tiny uniform pressure  $q$  on the membrane and the tension  $f$  on the membrane, as is shown in the following formula:

$$\frac{q}{f} = e^{\frac{i-1}{\beta}}, i = 1, 2, 3 \dots n \quad (18)$$

where  $\beta$  is a constant, which is determined by the material property of the elastic cylinder. The cylinder  $V$  of the membrane corresponding to the elastic cylinder material under the corresponding torque is:

$$V = \frac{1}{3} L \cdot S_c \quad (19)$$

where  $L$  is the changing length of the membrane in the  $Z$  axis direction of the membrane center point when the membrane is subjected to uniform pressure,  $S_c$  is the area of the irregular membrane, determined by the actual shape of the irregular elastic cylinder and the corresponding membrane shape.

### 3.4 The spatial change of key sample points

According to the computed displacement direction, the spatial variable quantity of the critical sample points under torque is computed.

After the irregular section of the elastic cylinder was twisted, twist angle of arbitrary section is in direct proportion to the vertical distance from the cross section to the fixed end. The twist angle of the cross section is  $H_i \cdot \theta_{A_k(H_i)}$  when the vertical angle of the cross section is  $H_i$  at the vertical distance from the fixed lower end.

At the initial position, the distance between the key sample points  $A_k(H_i)$  and the centroid  $o'$  of the cross section is  $r$ , as is shown in Fig. 4. In  $X, Y$  and  $Z$  directions, the coordinates are:  $X_{A_k(H_i)}, Y_{A_k(H_i)}, Z_{A_k(H_i)}$ . When twisting to the new position  $A'_k(H_i)$ , in the  $X, Y$  and  $Z$  direction, the coordinates are:  $X_{A'_k(H_i)}, Y_{A'_k(H_i)}$  and  $Z_{A'_k(H_i)}$ .

The angle between the segment connected by  $A_k(H_i)$  and  $o'$  and  $X$  is  $\alpha$ , and:

$$\alpha = \arcsin \frac{Y_{A_k(H_i)}}{r} \quad (20)$$

The variable quantity  $\Delta X_{A_k(H_i)}$  and  $\Delta Y_{A_k(H_i)}$  of the key sample point  $A_k(H_i)$  in the  $X$  and  $Y$  directions can be expressed as:

$$\Delta X_{A_k(H_i)} = X_{A'_k(H_i)} - X_{A_k(H_i)} = -r \cdot \sin \partial \cdot H_i \cdot \theta_{A_k(H_i)} = -Y_{A_k(H_i)} \cdot H_i \cdot \theta_{A_k(H_i)} \quad (21)$$

$$\Delta Y_{A_k(H_i)} = Y_{A'_k(H_i)} - Y_{A_k(H_i)} = r \cdot \cos \partial \cdot H_i \cdot \theta_{A_k(H_i)} = X_{A_k(H_i)} \cdot H_i \cdot \theta_{A_k(H_i)} \quad (22)$$

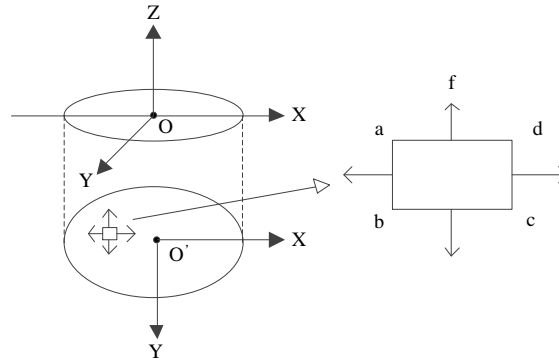


**Figure 4:** Mechanical sketch of micro membrane in membrane analogy

The key sample point  $A_k(H_i)$  is under the action of the torque  $M_T$ , the variable quantity in the  $Z$  axis direction is independent of the vertical distance  $H_i$  from the fixed end, then  $\Delta Z_{A_k}(H_i)$  is:

$$\Delta Z_{A_k}(H_i) = Z_{A'_k(H_i)} - Z_{A_k(H_i)} = \frac{2G\theta_{A_k(H_i)}fLh}{q\sqrt{X_{A_k(H_i)}^2 + Y_{A_k(H_i)}^2 + h^2}} \quad (23)$$

### 3.5 Cylinder model under twist action

According to the spatial variation of the critical sample points, the spatial position of the key sample points after twist is computed. We then update all points to build the twisted model. With such simulation method for free twist of elastic cylinder with irregular section, it is possible to obtain the estimated values  $\Delta X_{A_k}^*(H)$ ,  $\Delta Y_{A_k}^*(H)$  and  $\Delta Z_{A_k}^*(H)$  of the variable quantity in the  $X$ ,  $Y$  and  $Z$  axis directions on the  $K^{th}$  ridge. Similarly, estimated values can be obtained in the  $X$ ,  $Y$  and  $Z$  axis direction under the action of the torque  $M_T$  at any point on the other ridges on the side. The twisted elastic cylinder model was updated based on the estimated amount of any point change obtained on all the ridgelines.

## 4 Simulation system

In order to verify the model, a virtual operation simulation platform was built. The hardware system includes a PC system and a haptic equipment system. The configurations are: Intel i7 4.0 GHz CPU, 8 GB RAM, NVIDIA GeForce GTX 980 Ti graphics cards, LCD monitors, and PHANTOM OMNI haptic device of Sensible Technologies corp. The software consists of Windows system environment, VC++2016 and OpenGL graphical program interface. In this paper, the human stomach and arm were selected as the simulation objects of the model to do physical modeling and experimental verification. The simulation environment is shown in Fig. 5.

The simulation system consists of three modules: preprocessing, real-time simulation and user interface. The preprocessing module includes virtual scene initialization and haptic deformation model initialization. Virtual scene initialization includes 3D

modeling of virtual surgical instruments and 3D reconstruction using gastric and arm CT data [Cao, Zhou, Sun et al. (2018)]. Real-time simulation modules include collision detection and twisting models. The collision detection part is used to detect whether the surgical instrument has collided with the three-dimensional small intestine model. If there was a collision, the twist model would be loaded, otherwise we continue to track the position. The man-machine interaction module includes the interaction between the operator, the haptic interaction device and the display. The haptic interactive device outputs feedback of haptic information, and the display is refreshed by graphics, as is shown in Fig. 6.



**Figure 5:** Simulation environment

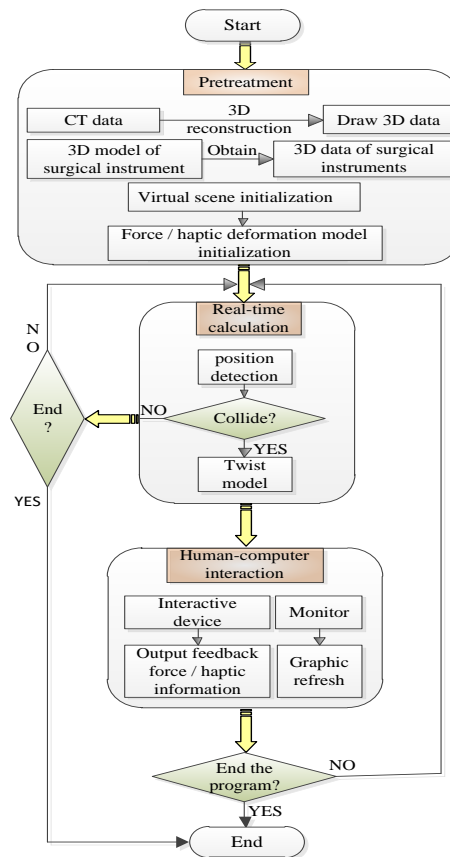


**Figure 6:** Flow chart

In the experimental platform, the same torque is applied to simulate the twist operation using the finite element model [Clark, Hoshizaki and Gilchrist (2018)] and the model in this paper, and the twist operation is performed at the same time. Compared with the model twist operation, we observe the better clarity and fluency of the entire picture. The stomach will change along the different axes simultaneously, or partially, due to abnormal morphogenetic transformation, according to different causes of gastric twist. There are mainly four kinds of common twist mode, as is shown in Fig. 7. Our simulation model and finite element model of the stomach are shown in Fig. 8 and Fig. 9. The experimental results show that there are no burr and rough edges in the deformation edges of our model. In human-computer interaction process, it can accurately express the immersion of the virtual visual and haptic sense on body and meet the real-time requirement. After the operation, the texture of the stomach image is clear, the visual perception is plausible, and the picture quality is superior to the finite element model.

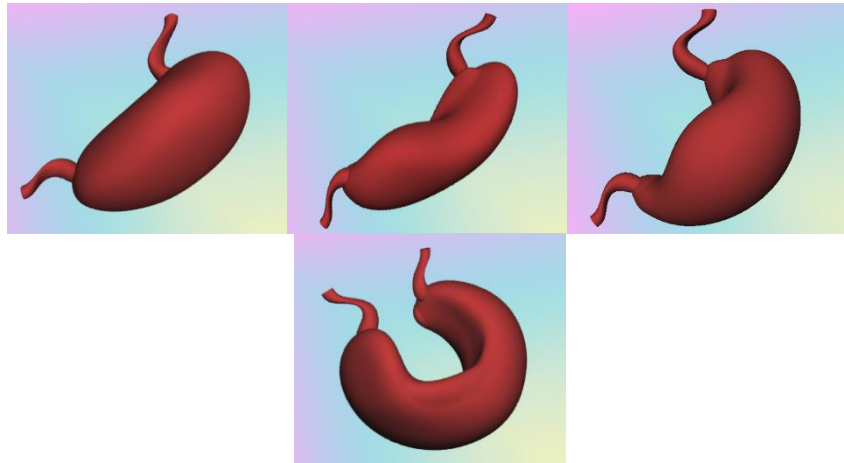


**Figure 7:** Four common patterns of gastric twist

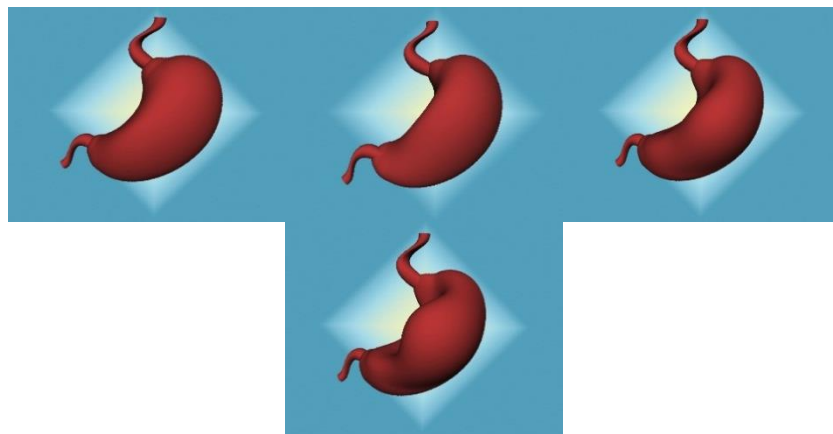


**Figure 8:** The gastric twist process of the proposed model

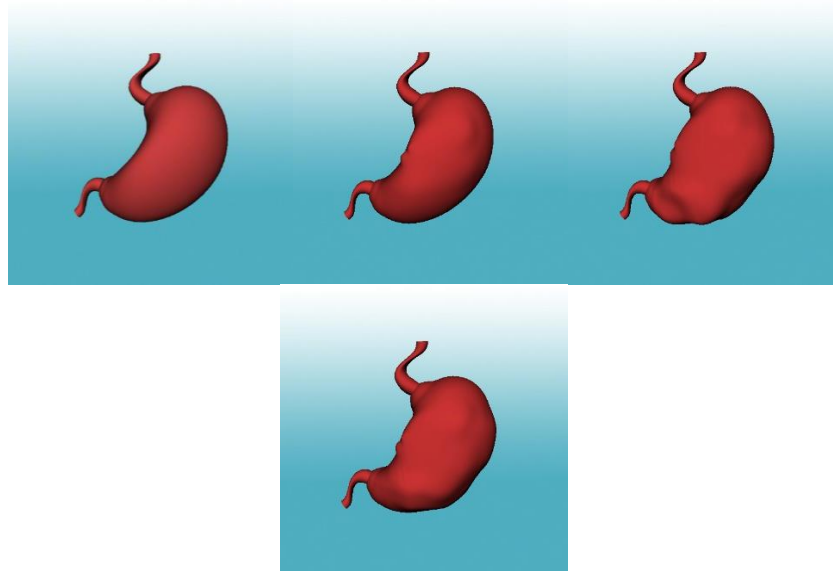


**Figure 9:** The gastric twist process of finite element model

## **5 Discussions**

In order to verify the real-time performance and accuracy of the model, the experimental model is compared with the finite element model and the mass-spring model respectively in terms of the deformation time and the deformation accuracy. The performance evaluation method is designed and the experimental results are analyzed. Finally, several physicians are invited to use the system to score the training results. The experimental results showed that the system has good training effects.

### **5.1 Simulation time**

Due to the large amount of data in the interactive operation of virtual simulation operation, the speed of deformation becomes the fundamental requirement of virtual surgery. The membrane analogy method models the small grid of the surface as a membrane, and implements force analysis of the small membrane, as well as accurately calculates the displacement of the twist deformation, which improves the operation efficiency. The real-time requirement means that time consumed on the operation should be within human's sensory error. Same-sized torque is used to twist the simulated stomach established by mass-spring model (MSM) [Ansari and Mahmoudinezhad (2015)], the finite element model (FEM) the proposed model (PM) and real wrist (RW) in the same experimental environment. The real-time difference was compared in the time of visualization after virtual twist operation. The experimental results are shown in Fig. 10.

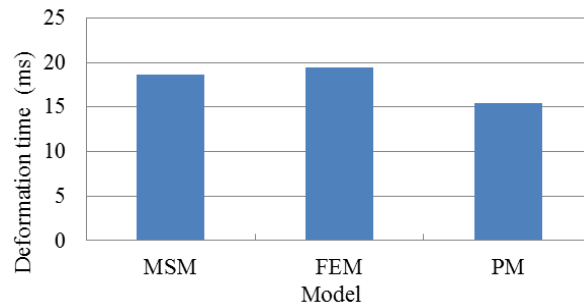


**Figure 10:** Deformation time of different models

The experiment results show that, the model saves deformation time by using the Kriging interpolation to interpolate the rest soft tissue through the acquisition of key sample points. Then the membrane analogy method is used for twist. The stress surface is decomposed into small pieces of membrane for force analysis, which can accurately compute the space deformation of the soft tissue. The combination of the two methods promotes computation efficiency to avoid large computation consumption. The total time required to complete the twist of our model is shorter than those of the finite element model and the mass-spring model, indicating that the model has better real time performance.

### 5.2 The twist accuracy

The higher the accuracy in operation, the better in simulation. In order to verify the accuracy of the model in a wide range of deformation, we set the following experiment. In the same experimental environment, we set the length of the virtual wrist, the thickness and the length of the finger are same with the real wrist parameters. According to the wrist shape characteristics, we select the 10 specific markers of the basic parts of the wrist to mark the virtual wrist and the real wrist (RW), as is shown in Fig. 11. We record the displacement of the twist when the situation is completed. The arm twist process is shown in Fig. 12.

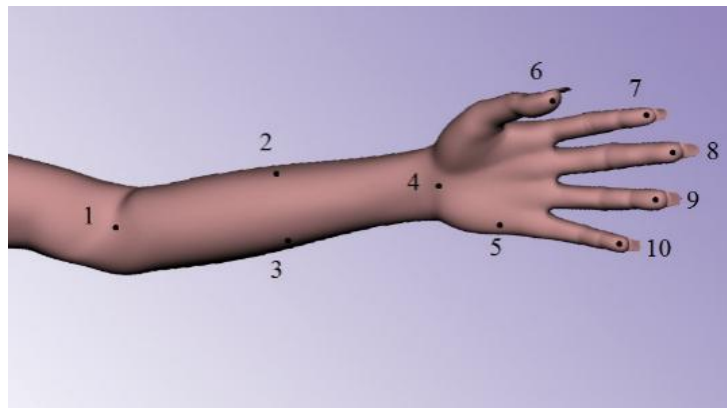


**Figure 11:** Position of the 10 specific markers

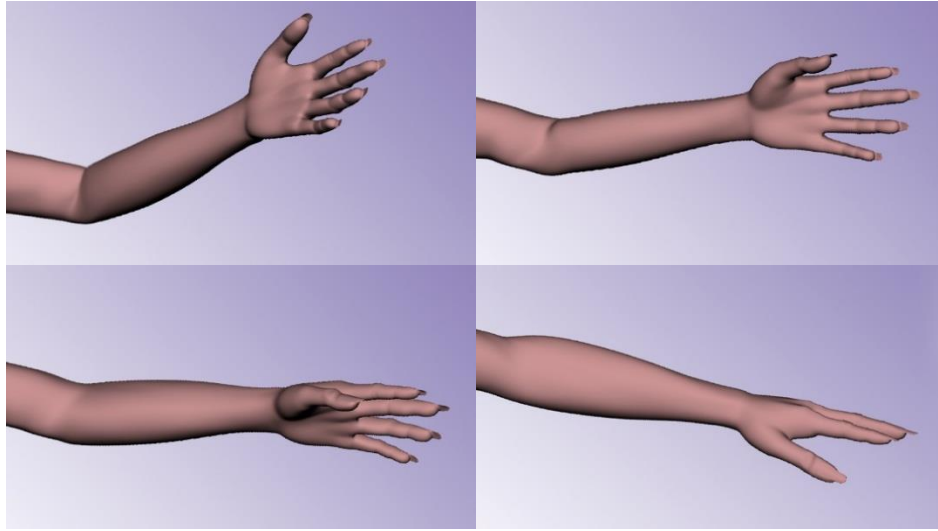


**Figure 12:** Arm model twist process

The 3D coordinate of each point in the initial state of the wrist is recorded as  $O_i(x_0, y_0, z_0)$ , the coordinate marker is  $O'_i(x_1, y_1, z_1)$  after the end of the twist operation, the displacement  $D$  is:

$$D = \sqrt{(x_1 - x_0)^2 + (y_1 - y_0)^2 + (z_1 - z_0)^2} \tag{24}$$

The results of the twist displacement experiment for each marker point were shown in Fig. 13. Data showed that the difference between virtual wrist simulated by our model and the real wrist at the mark points is smaller than that of the other two models, indicating that the model is more accurate.

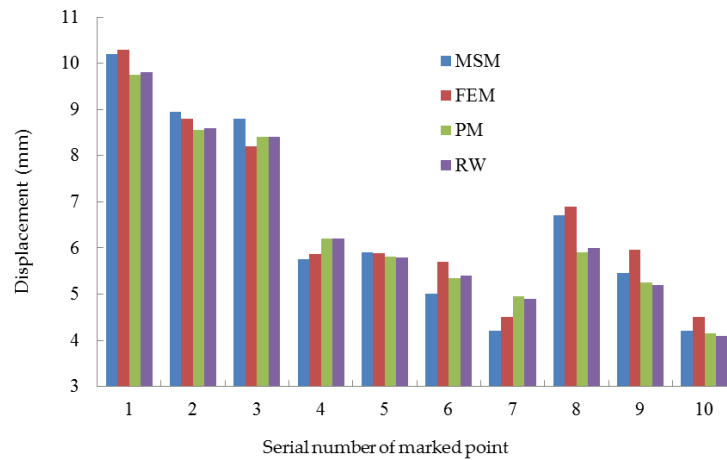


**Figure 13:** Model displacement

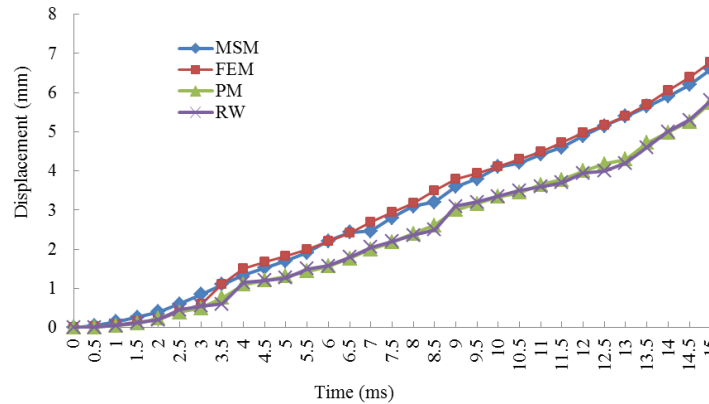


**Figure 14:** Comparison of marker points during torsion

To study the accuracy of the process, taking the No. 8 marker as a point of interest, the change of the displacement with time is recorded during the reversing operation. Using the same torque on the finite element model, this model and the real wrist were twisted, respectively, as is shown in Fig. 14. The experimental results showed that, in the whole process of twist, the displacement difference between our model and the real wrist is smaller than that of the finite element model and the mass-spring model, which indicates the model in the process of twist simulation has better accuracy.

### 5.3 Model comprehensive performance

To objectively verify the performance of the model, the weighted comprehensive evaluation method was adopted. We select nine evaluation indicators that can characterize the model best: effectiveness, force feedback, real-time performance, system stability, deformation efficiency, fidelity, image fluency, telepresence and texture which were numbered from 1 to 9. When evaluating the model, the index weights were: 0.15, 0.15, 0.15, 0.15, 0.1, 0.1, 0.1, 0.05, 0.05 in Tab. 1. In this paper, the twist model is compared with the classical mass-spring model and the finite element model.

**Table 1:** Index weights

No.	Index	weight
1	Effectiveness	0.15
2	force feedback	0.15
3	real-time performance	0.15
4	system stability	0.15
5	deformation efficiency	0.1
6	Fidelity	0.1
7	image fluency	0.1
8	Telepresence	0.05
9	Texture	0.05

Forty physicians were randomly selected from the First Affiliated Hospital of Nanjing Medical University, including 20 interns, A (male, 7 female, 13), with an average age of 23; 10 deputy chief physicians B (male, 6 female, 4), with an average age of 30; 10 chief physicians C (male, 7 female, 3), with an average age of 46. Among them, the weight of each score is 0.2, 0.3 and 0.5 respectively. The interns interacted with the virtual wrist by the hand controller, and chief physicians communicated with the interns after the experimental experience. The system indicators are evaluated after each trial. The scores are from 0 to 10 points. By comparing the experimental results, higher weighted average score indicates that the model has better performance.

Each evaluation index  $M$  is divided into:

$$M = 20\% \cdot \left(\sum_{i=1}^{20} A_i / 20\right) + 30\% \cdot \left(\sum_{i=1}^{10} B_i / 10\right) + 50\% \cdot \left(\sum_{i=1}^{10} C_i / 10\right) \quad (25)$$

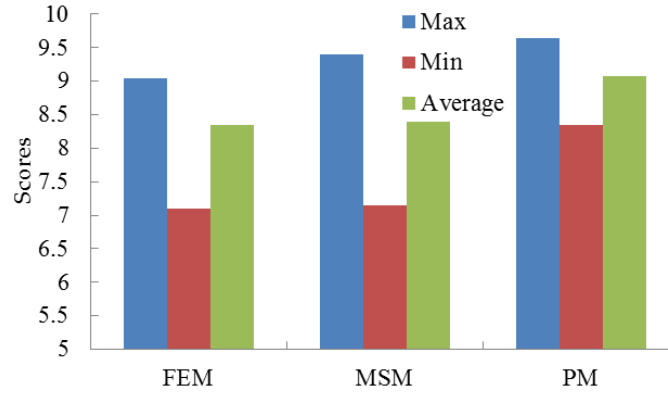


**Figure 15:** Comparison chart of model evaluation

As is shown in Fig. 15, the lowest and the highest scores of the proposed model are higher than the other two models, and the average score is also higher than the other two models. The experimental data shows that the model has better performance.

The variance  $s_j^2$  of each evaluation index is:

$$s_j^2 = \frac{1}{A+B+C} \sum_{i=1}^{40} (x_i - M_j)^2 \quad (26)$$

Where  $x_i$  is the  $i^{th}$  chief physician's scores on the model, and  $M_j$  is the average of the  $j^{th}$  evaluation index.

Each model's comprehensive score that combined with the evaluation of the indicators is:

$$N = \sum_{i=1}^4 (15\% \cdot M_i) + \sum_{i=5}^7 (10\% \cdot M_i) + \sum_{i=8}^9 (5\% \cdot M_i) \quad (27)$$

where  $M_i$  is the average score of the  $i^{th}$  evaluation criteria.

We compare the experimental results using the weighted average score  $M$  and the variance  $s^2$ . The average score and variance of the three models were shown in Fig. 16

and Fig. 17. The scores from the chief physicians were shown in Fig. 18. The comprehensive scores were also shown as box diagrams in Fig. 19.

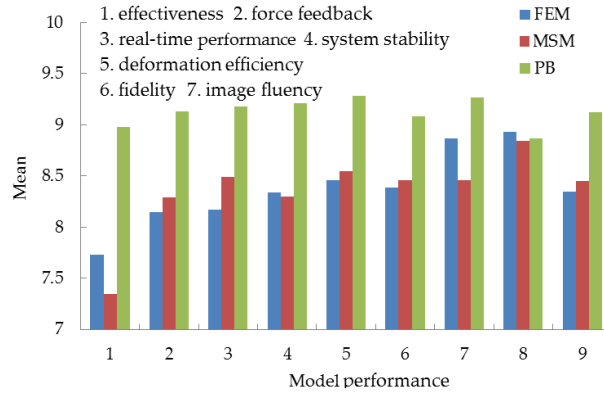


**Figure 16:** Comparison chart of average score

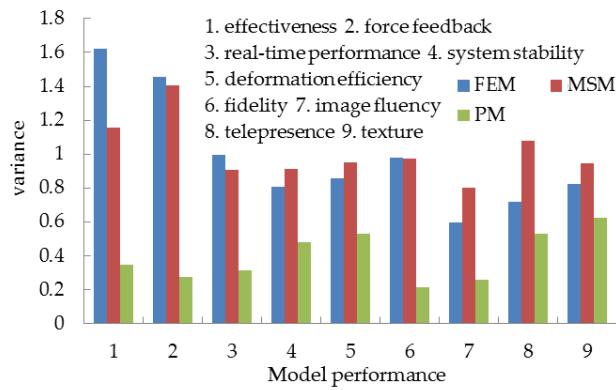


**Figure 17:** Comparison chart of variance

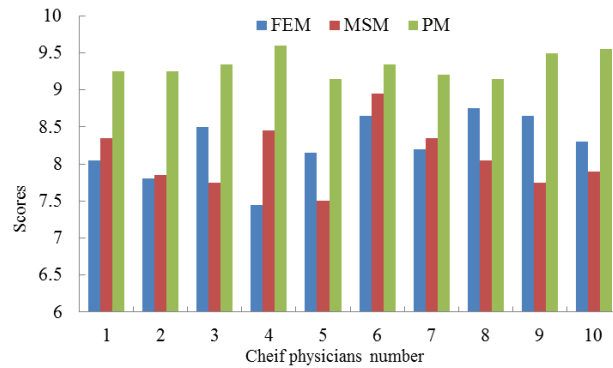


**Figure 18:** Chart of model comprehensive evaluation

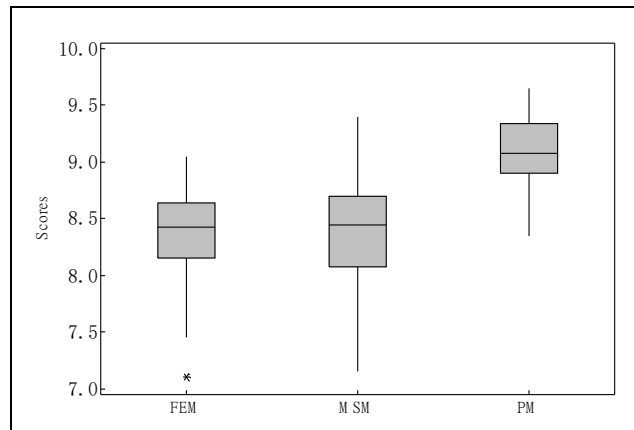


**Figure 19:** Comparison chart of model comprehensive evaluation

The experimental results showed that the proposed model is better than the other two models. The small variance showed that the comprehensive stability of the proposed system is higher. The model has obvious advantages in telepresence, texture, real-time performance, validity and system stability. The superior telepresence and texture characteristics give the operator the feeling like the actual operation of the same object. This makes the training more realistic, accurate and reliable, and ensures the convergence and completeness of the model. Real-time performance, effectiveness and system stability verifies that the model produces more realistic deformation. The simple algorithm in the process of deformation can meet the requirements of the authenticity, stability and real-time performance of the interactive system.

## 6 Discussions

To verify the application of the proposed model, 30 interns (17 male, 13 female) and 10 surgical chief physicians (7 male, 3 female) were randomly selected in the First Affiliated Hospital of Nanjing Medical University, the average age of interns was 24 years old from graduate freshmen to doctoral student, including 7 male and 3 female interns. Interns carried out the experimental operation and the chief physician evaluated on its operation process. Thirty interns were randomly divided into three groups, each group has 10 interns and they are numbered from 1 to 10. The first group used this virtual platform to do a 40 min virtual arm twisting experiment. The second group used this virtual platform to do a 20 min twist training and then do a 20 min real arm twisting experiment. The third group trained 40 min twist experiment with a real arm. Each group of training staff can interrupt in the period of training to rest for 5 min if they want.

20 min and 40 min before the experimental training, 30 interns were separately evaluated by 10 chief physicians when interns are twisting the actual arm according to the training time, proficiency, operational accuracy and other indicators of interns' twist operation. The score ranges from 1 to 10. The score of every intern is computed from as the average score from the 10 chief physicians. Only four operators in the trial had a break, the other operators had no interruption.

The pre-training evaluation results of interns that participated are shown in Fig. 20. Because there is no relevant twist operation experience, the operators' scores in the three groups are generally low and had little difference. We tested the trainees after they had used our system for 20 min. The first group and the second group were training in virtual arm torsion, and the third group was training in real arm torsion. Results showed that the scores of the first and second group were slightly higher than the third group on real arm twisting. However, because they did not carry out the twist operation training on the real arm, they did not grasp the relevant essentials. The score gap was not obvious, as is shown in Fig. 21. After 40 min, the training results of the three groups were shown in Fig. 22. As the second group after several virtual trainings and the second half of the time in real training, the score was significantly higher than the other two groups. The first group took more virtual training than the others but did not carry out real arm twist training, so the score was slightly higher than the third group.

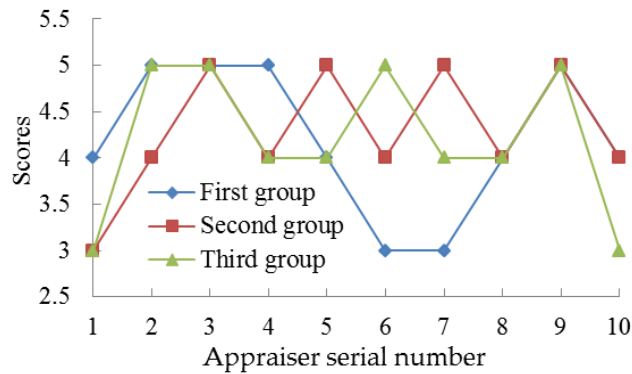


**Figure 20:** Evaluation on interns before the training

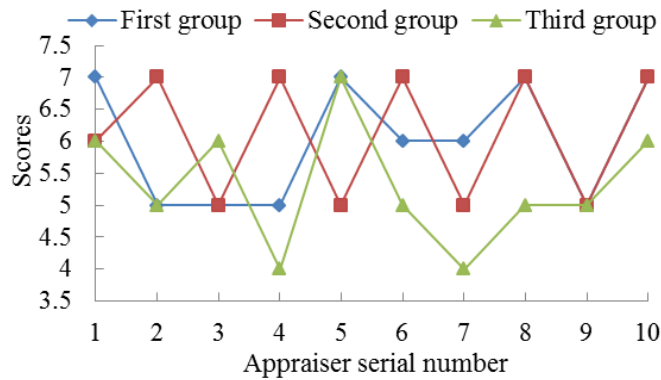


**Figure 21:** Evaluation on interns at the middle time of the training

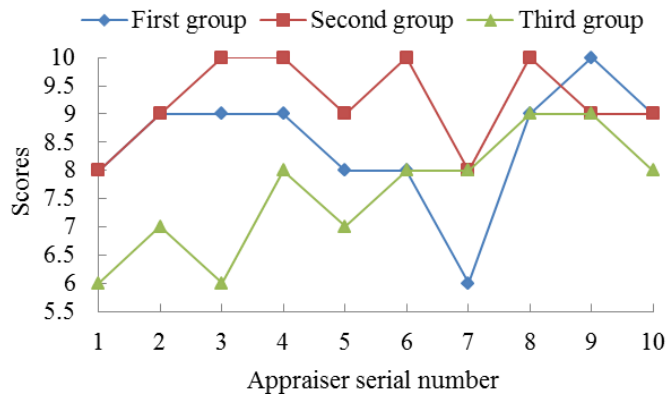


**Figure 22:** Evaluation on interns after the training

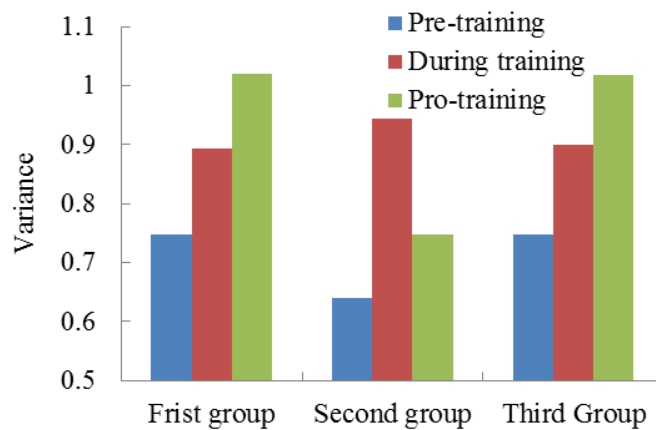


**Figure 23:** Variance of training evaluation

The evaluation score variance was shown in Fig. 23. The experimental results showed that due to training of virtual surgery, with higher training frequency, supplemented by a real arm experiment, the experiment can achieve better training results. Interns who practiced on the virtual twist operation in this system before using the real arm to twist always had better performance and operated more skillfully and accurately.

In conclusion, we propose a Kriging interpolation and membrane analogy method to study the simulation of free twist deformation of virtual arm and gastric. It is used to simulate the deformation process of small intestine tissue in virtual reality. Using OpenGL and VC++2016, the stomach and arm model training system for twist operation was built with PHANTOM OMNI haptic interaction device. In this method, the displacement tangent to the cross section of the irregular elastic cylinder under the twisting action is computed by combining the membrane analogy and the kriging interpolation methods, so that the amount of twist deformation can be computed intuitively, accurately and quickly. Real-time deformation simulation of elastic tissue is also guaranteed, and the accuracy of virtual haptic interaction can be improved. In order to verify the accuracy of the model, we design a multi-point positioning comparison

method in experiment. The experimental results show that our twist model has a good real-time performance, stability and is suitable for telepresence.

**Acknowledgement:** This work was supported in part by the National Nature Science Foundation of China (No. 61502240, 61502096, 61304205, 61773219), Natural Science Foundation of Jiangsu Province (BK20150634, BK20141002).

## References

- Ansari, R.; Mahmoudinezhad, E.** (2015): Characterizing the mechanical properties of carbon nanocones using an accurate spring-mass model. *Computational Materials Science*, vol. 101, pp. 260-266.
- Benítez, J. M.; Montáns, F. J.** (2017): The mechanical behavior of skin: Structures and models for the finite element analysis. *Computers & Structures*, vol. 190, pp. 75-107.
- Cao, Y.; Zhou, Z.; Sun, X.; Gao, C.** (2018): Coverless information hiding based on the molecular structure images of material. *Computers, Materials & Continua*, vol. 54, no. 2, pp. 197-207.
- Chen, C.; Liu, F.; Li, Y.; Yan, C.; Liu G.** (2016): A robust interpolation method for constructing digital elevation models from remote sensing data. *Geomorphology*, vol. 268, pp. 275-287.
- Clark, J. M.; Hoshizaki, T. B.; Gilchrist, M. D.** (2018): Assessing women's lacrosse head impacts using finite element modelling. *Journal of the Mechanical Behavior of Biomedical Materials*, vol. 80, pp. 20-26.
- Dehghan, M. Abbaszadeh, M.** (2017): Two meshless procedures: moving Kriging interpolation and element-free Galerkin for fractional PDEs. *Applicable Analysis*, vol. 96, pp. 936-969.
- Ganganagoudar, A.; Mondal, T. G.; Prakash, S. S.** (2016a): An improved morphological algorithm for filtering airborne lidar point cloud based on multi-level kriging interpolation. *Remote Sensing*, vol. 8, no. 35, pp. 1-15.
- Ganganagoudar, A.; Mondal, T. G.; Prakash, S. S.** (2016b): Analytical and finite element studies on behavior of FRP strengthened RC beams under torsion. *Composite Structures*, vol. 153, pp. 876-885.
- Kim, Y.; Chang, D.; Kim, J.; Park, S.** (2013): Gallbladder removal simulation for laparoscopic surgery training, a hybrid modeling method. *Journal of Computer Science and Technology*, vol. 28, pp. 499-507.
- Liu, Y.; Yu, J.; Shen, Y.; Lv, X. Q.** (2016): A modified interpolation method for surface total nitrogen in the Bohai Sea. *Journal of Atmospheric and Oceanic Technology*, vol. 33, pp. 1509-1517.
- Spranger, K.; Capelli, C.; Bosi, G. M.; Schievano, S.; Ventikos, Y.** (2015): Comparison and calibration of a real-time virtual stenting algorithm using finite element analysis and genetic algorithms. *Computer Methods in Applied Mechanics and Engineering*, vol. 293, pp. 462-480.

**Surkay D. A.; Mahir, A. M.** (2018): The interface stress field in the elastic system consisting of the hollow cylinder and surrounding elastic medium under 3D non-axisymmetric forced vibration. *Computers, Materials & Continua*, vol. 54, no. 1, pp. 61-81.

**Troyani, N.; Pérez, A.; Gomes, C.; Baíz, P.; Fonseca, Z. D.** (2009): Selective finite element refinement in torsional problems based on the membrane analogy. *Finite Elements in Analysis and Design*, vol. 45, pp. 547-554.

**Tu, S.; Dong, L.; Yang, H.; Huang, Y.** (2016): Complex variable moving Kriging interpolation for boundary meshless method. *Engineering Analysis with Boundary Elements*, vol. 65, pp. 72-78.

**Yang, W.; Yuan, H.; Zhao, T.** (2017): Multi-field coupling dynamic characteristics based on Kriging interpolation method. *Proceedings of the Institution of Mechanical Engineers, Part G: Journal of Aerospace Engineering*, vol. 231, pp. 1088-1099.

**Zhang, X.; Gao, R.; Yan, R.; Chen, X.; Sun, C. et al.** (2016): B-spline wavelet on interval finite element method for static and vibration analysis of stiffened flexible thin plate. *Computers, Materials & Continua*, vol. 52, no. 1, pp. 53-71.